A&A 391, 917–922 (2002)
DOI: 10.1051/0004-6361:20020969

Astronomy & Astrophysics

Research Note

Radio luminosities and classificatory criteria of BL Lacertae objects

D. C. Mei, L. Zhang, and Z. J. Jiang

Department of Physics, Yunnan University, Kunming 650091, PR China

Received 17 April 2002 / Accepted 26 June 2002

Abstract. Using the sample of radio-selected BL Lacertae objects (RBLs) and X-ray selected BL Lacertae objects (XBLs) presented by Sambruna et al. (1996), we calculated the luminosities in radio, optical and X-ray of each source and made a statistical analysis among the luminosities at different wave-bands, broad-band spectral indices from radio to X-ray ($\alpha_{\rm rx}$) and peak frequencies ($\nu_{\rm p}$). Our results are as follows: (i) there is a positive correlation between radio luminosity $L_{\rm r}$ and $\alpha_{\rm rx}$ and a negative correlation between $L_{\rm r}$ and $\nu_{\rm p}$. High-energy peak BL Lacs (HBLs) and low-energy peak BL Lacs (LBLs) can be distinguished very well; the dividing lines are probably those of $\log L_{\rm r} = 43.25$ (erg/s) and $\alpha_{\rm rx} >$(or $\leq$)0.75 for $\log L_{\rm r}$–$\alpha_{\rm rx}$ plot and those of $\log L_{\rm r} \leq 43.25$ (erg/s) and $\log \nu_{\rm p} > 14.7$ for the $\log L_{\rm r} - \log \nu_{\rm p}$ plot; (ii) there is a weak positive correlation between optical luminosity $L_{\rm o}$ and $\alpha_{\rm rx}$ and a negative weak correlation between $L_{\rm o}$ and $\nu_{\rm p}$; (iii) there is no correlation between X-ray luminosity $L_{\rm x}$ and $\alpha_{\rm rx}$ or between $L_{\rm x}$ and $\nu_{\rm p}$. From our analysis, we find that synchrotron radiation is the main X-ray radiation mechanism for HBLs while inverse Compton scattering is dominant for LBLs.

Key words. galaxies: BL Lacertae objects: general – galaxies: fundamental parameters – radiation mechanism: non–thermal

Most BL Lac objects have been identified in either radio surveys (radio-selected BL Lac objects (RBLs)) or X-ray surveys (X-ray-selected BL Lac objects (XBLs)). These two kinds of BL Lac objects show many significant differences (for example see Ledden & O'Dell 1985; Ghisellini et al. 1986; Stocke et al. 1991). The main differences between RBLs and XBLs are as follows. First, there is a difference in spectral energy distributions (SEDs); RBL–like objects show $\alpha_{\rm rx} > 0.75$, while XBL-like objects show $\alpha_{\rm rx} \leq 0.75$ (see, e.g., Ledden & O'Dell 1985; Stocke et al. 1985; Giommi et al. 1990; Stocke et al. 1991; Schachter et al. 1993; Giommi & Padovani 1994). It should be pointed out that Padovani & Giommi (1995) introduced the distinction between high-energy peak BL Lacs (HBLs) and low-energy peak BL Lacs (LBLs), for objects which emit most of their synchrotron power at high (UV-soft-X) and low (far-IR, optical) frequencies respectively. However, a quantitative distinction can be drawn on the basis of the ratio between radio and X-ray fluxes. It can also use the broad-band spectral index $\alpha_{\rm rx}$ to distinguish HBLs and LBLs: $\alpha_{\rm rx} \leq 0.75$ for HBLs and $\alpha_{\rm rx} > 0.75$ for LBLs (Giommi et al. 1995). Secondly, there is a difference in the peak frequency distributions (Giommi et al. 1995; Padovani & Giommi 1995; Urry & Padovani 1995; Padovani & Giommi 1996; Lamer et al. 1996). Sambruna et al. (1996) made a parabolic fit to multi-band flux data to obtain the peak frequency of the synchrotron emission, $\nu_{\rm p}$, of sources, when studying quantitatively how the peak-emission frequency of the synchrotron emission can be used to distinguish RBL–like and XBL–like objects. Making use of the peak frequency, $\nu_{\rm p}$, of the synchrotron emission estimated by Sambruna et al. (1996). Qin et al. (1999) found that, in the four different regions divided by the $a_{\rm rx} = 0.75$ line and the $\log \nu_{\rm p} = 14.7$ line, all RBL–like objects lie in the upper left region, while most XBL–like objects are within the lower right region, with only a few sources being located in the lower left region and no sources being located in the upper right region. Considering the proper physical origin of the X-ray emission for different classes of BL Lac objects, we calculated the peak frequency $\nu_{\rm p}$ of the synchrotron emission of each source in the sample of Sambruna et al. (1996). It was found that all RBL-like objects, defined by $\alpha_{\rm rx} > 0.75$, are located in the upper-left region, while all XBL-like objects, defined by $\alpha_{\rm rx} \leq 0.75$, are inside the lower-right region. No sources are in the lower left and upper-right regions, suggesting that the classification criterion in terms of the peak frequency should be $\log \nu_{\rm p} = 14.7$ and the classification criterion of $\alpha_{\rm rx}$ is equal to the classification criterion of $\log \nu_{\rm p}$ (Dong et al. 2002). This provides evidence supporting what Giommi et al. (1995) proposed: RBL-like and XBL-like objects can be distinguished by the difference in the peak frequency of the synchrotron emission.

Sambruna et al. (1996) found that the position of the peak frequency $\log \nu_{\rm p}$ is linked to the luminosity. For more luminous objects, the peak of the synchrotron power is located at lower frequencies. Fossati et al. (1998) studied the spectral energy distributions of three subclass samples of blazars. They also found that despite the differences in continuum shapes for subclasses of blazars, a unified scheme is possible; blazar continua can be described by luminosity as a fundamental parameter.

Send offprint requests to: D. C. Mei,
e-mail: kmdcmei@public.km.yn.cn

Table 1. Sample of X-ray selected BL lacertae objects (XBLs).

Name	z^*	α^*_{rx}	F^*_r(Jy) (5 GHz)	F^*_o(mJy) (5500 Å)	F^*_x(μJy) (1 keV)	$\log \nu^\#_p$ (Hz)
0112.1+0903	0.339	0.58	0.0014	0.047 ± 0.001	0.05	15.62
0158.5+0019	0.299	0.51	0.0113	0.21 ± 0.06	1.2	17.34
0205.7+3509	0.318	0.46	0.0036	0.10 ± 0.005	0.90	18.06
0257.9+3429	0.247	0.65	0.010	0.25 ± 0.02	0.10	15.03
0317.0+1834	0.190	0.58	0.017	0.36 ± 0.09	0.54	15.79
0419.3+1943	0.512	0.53	0.008	0.09	0.75	18.31
0607.9+7108	0.267	0.70	0.0182	0.09	0.07	15.23
0737.9+7441	0.315	0.56	0.024	0.64	1.30	16.09
0922.9+7459	0.638	0.55	0.0033	0.044 ± 0.002	0.21	17.21
0950.9+4929	0.207	0.51	0.0033	0.122 ± 0.04	0.27	16.13
1019.0+5139	0.141	0.45	0.0024	0.22	0.93	16.69
1207.9+3945	0.615	0.52	0.0058	0.10	0.55	17.38
1221.8+2452	0.218	0.67	0.0264	0.42 ± 0.09	0.18	15.00
1229.2+6430	0.164	0.56	0.042	0.55 ± 0.17	2.05	16.71
1235.4+6315	0.297	0.55	0.007	0.14 ± 0.02	0.31	16.16
1402.3+0416	0.200	0.57	0.0208	0.88 ± 0.37	0.68	15.39
1407.9+5954	0.495	0.66	0.0165	0.07 ± 0.01	0.10	15.76
1443.5+6349	0.299	0.58	0.0116	0.06	0.35	17.71
1458.8+2249	0.235	0.58	0.0298	1.01 ± 0.20	0.78	15.39
1534.8+0148	0.312	0.61	0.034	0.15 ± 0.05	0.74	17.40
1552.1+2020	0.222	0.54	0.0375	0.44 ± 0.08	2.57	17.45
1757.7+7034	0.407	0.50	0.0072	0.18	0.92	17.15
2143.3+0704	0.237	0.61	0.050	0.32 ± 0.04	0.78	16.24

* These data are taken from Tables 1 and 2 of Sambruna et al. (1996).
# These data are taken from Table 1 of Dong et al. (2002).

In this paper, we will study how the luminosity of each energy band can be used to distinguish RBLs and XBLs. We calculated the luminosity of each energy band for RBLs and XBLs presented in Table 1 of Sambruna et al. (1996) in Sect. 2. We present our analysis results in Sect. 3, and give our discussion and conclusions in Sect. 4.

1. Luminosity of BL Lac objects

We calculated the luminosities for the sample of RBLs and XBLs presented by Sambruna et al. (1996). We list the names, red-shifts, broad-band spectral indices, the energy fluxes at radio, optical and X-ray bands and peak frequencies of 23 XBLs in Table 1 and 29 RBLs in Table 2, respectively. Using the logrithmic parabolic form given by Laudau et al. (1986) and the data of the energy fluxes at radio, optical and X-ray bands, Dong et al. (2002) calculated the peak frequencies of 23 XBLs in Table 1 which are used here. Sambruna et al. (1996) made a parabolic fit to the radio, millimeter, IR, optical, and X-ray fluxes data to obtain the peak frequency, ν_p, of the spectral energy, where, for some XBLs, X–ray data were not included in the fit. The data of peak frequency ν_p, of the synchrotron emission in Table 2 make use of Sambruna et al. (1996) except for objects 1652+398 and 2005−489, because both sources are HBLs ($\alpha_{rx} < 0.75$). We use the ν_p data of two sources calculated by Dong et al. (2002). Therefore, in our sample, there are 27 LBLs that consist of RBLs except for 1652+398 and 2005−489 in Table 2 and 25 HBLs that consist of 23 XBLs and two RBLs (1652+398 and 2005−489).

We calculated rest-frame luminosities of radio, optical and X-ray energy bands using the fluxes of BL Lac objects in Tables 1 and 2. For the K-correction, the flux densities were multiplied by $(1+z)^{\alpha-1}$, where α is the power-law spectral index in the appropriate energy band ($F_\nu \propto \nu^{-\alpha}$). For RBLs, we used $\alpha_r = 0.2$, and $\alpha_{opt} = 1.05$ (Falomo et al. 1994), while for XBLs we used $\alpha_r = 0$ and $\alpha_{opt} = 0.65$ (Falomo et al. 1994). We used individual spectral indices in the X-ray provided by Sambruna et al. (1996). The redshifts of 0048−097, 1147+245 and 1519−273 presented in Table 2 of Sambruna et al. (1996) are not available. A mean value of $z = 0.56$ is accordingly adopted for these sources. The flux densities were converted to luminosities using $H_0 = 75$ km s^{-1} Mpc^{-1} and $q_0 = 0.5$, assuming isotropic emission. We calculated the radio luminosity L_r, optical luminosity L_o and X-ray luminosity L_x in rest frame.

2. Results

We now consider the relations among radio luminosity, broad-band spectral index and peak frequency. We plot L_r versus α_{rx} in Fig. 1a, which shows that the radio luminosity increases as the broad-band spectrum index increases. A linear regression analysis yields

$$\log L_r = (6.64 \pm 0.49)\alpha_{rx} + (38.24 \pm 0.37), \quad (1)$$

Table 2. Sample of radio selected BL lacertae objects (RBLs).

Name	z^*	α_{rx}^*	F_r^*(Jy) (5 GHz)	F_o^*(mJy) (5500 Å)	$F_x^*(\mu$Jy) (1 keV)	$\log \nu_p{}^*$ (Hz)
0048−097	...	0.75	1.110 ± 0.583	2.41 ± 1.63	0.77	13.84
0118−272	>0.557	0.86	1.145 ± 0.075	1.92 ± 0.38	0.20	14.49
0235+164	0.940	0.76	1.81 ± 0.54	1.44 ± 1.06	1.56	13.39
0426−380	>1.030	0.90	1.15 ± 0.03	0.11	0.09	13.22
0454+844	0.112	1.01	1.41 ± 0.14	0.70 ± 0.36	0.02	13.81
0537−441	0.896	0.82	3.93 ± 0.17	1.49 ± 0.43	0.78	14.07
0716+714	>0.300	0.75	0.86 ± 0.18	2.96	1.17	13.79
0735+178	>0.424	0.88	2.13 ± 0.50	3.22 ± 1.56	0.22	14.03
0814+425	0.258	0.98	1.86 ± 0.68	0.26 ± 0.04	0.05	13.34
0851+202	0.306	0.84	2.99 ± 0.56	6.08 ± 5.91	0.70 ± 0.25	13.72
0954+658	0.367	0.88	0.90 ± 0.38	0.86 ± 0.24	0.16	14.09
1144−379	1.048	0.82	1.61 ± 0.96	0.62 ± 0.37	0.41	13.75
1147+245	...	0.92	0.82 ± 0.12	1.53 ± 0.36	0.05	14.58
1308+326	0.997	0.91	2.26 ± 0.40	2.23 ± 1.53	0.13	13.83
1418+546	0.152	0.85	1.22 ± 0.38	2.72 ± 0.82	0.30	13.85
1519−273	...	0.86	2.17 ± 0.25	0.47 ± 0.35	0.39	13.17
1538+149	0.605	0.93	1.53 ± 0.42	0.32 ± 0.10	0.09	13.56
1652+398	0.033	0.67	1.27 ± 0.10	15.65 ± 4.52	8.30	15.01
1749+096	0.320	0.92	1.44 ± 0.36	1.18 ± 0.54	0.14 ± 0.01	13.27
1749+701	0.770	0.81	1.11 ± 0.35	0.99 ± 0.22	0.15	14.43
1803+784	0.679	0.88	2.79 ± 0.30	0.99 ± 0.22	0.26 ± 0.03	13.43
1807+698	0.051	0.87	1.71 ± 0.32	7.85 ± 2.44	0.32	14.26
1823+568	0.664	0.85	1.45 ± 0.21	0.17	0.42	13.65
2005−489	0.071	0.71	1.21 ± 0.02	9.85 ± 1.71	4.12 ± 1.77	14.86
2007+777	0.342	0.91	1.72 ± 0.41	1.17 ± 0.18	0.17	13.66
2131−021	0.557?	0.96	1.84 ± 0.31	0.16 ± 0.04	0.05	13.16
2200+420	0.069	0.85	2.14 ± 0.66	8.65 ± 4.62	0.88	14.25
2240−260	0.774	0.89	1.03	0.26 ± 0.10	0.07	13.32
2254+074	0.190	0.88	0.56 ± 0.27	0.60 ± 0.19	0.09	13.25

* These data are taken from Tables 1 and 2 of Sambruna et al. (1996).

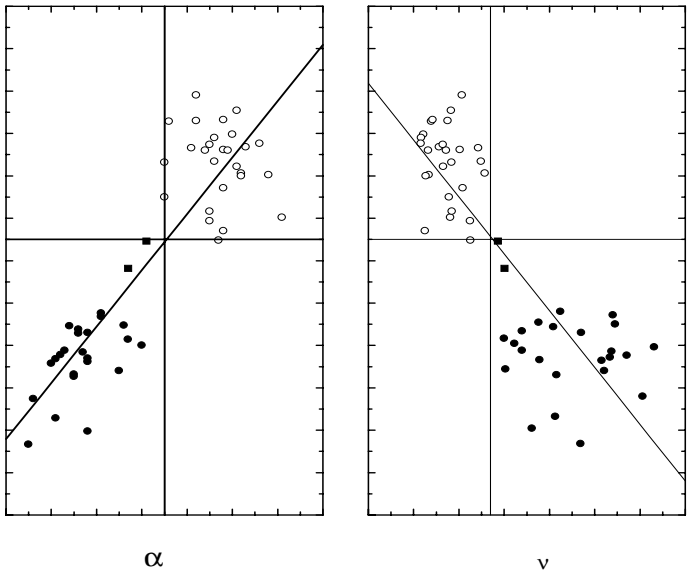

Fig. 1. a) Plot of $\log L_r - \alpha_{rx}$ for RBL and XBL samples. The empty circles represent RBLs, solid squares represent 1652+398 and 2005−489, and the solid circles represent XBLs. The horizontal solid line is $\alpha_{rx} = 0.75$ and the vertical solid line is $\log L_r = 43.25$. The oblique solid line is the regression line $\log L_r = (6.64 \pm 0.49)\alpha_{rx} + (38.24 \pm 0.37)$; **b)** plot of $\log L_r - \log \nu_p$ for RBL and XBL samples. The empty circles represent RBLs, solid squares represent 1652+398 and 2005−489, and the solid circles represent XBLs. The horizontal solid line is $\log \nu_p = 14.7$ and the vertical solid line is $\log L_r = 43.25$. The oblique solid line is the regression line $\log L_r = -(0.67 \pm 0.06) \log \nu_p + (53.13 \pm 0.92)$.

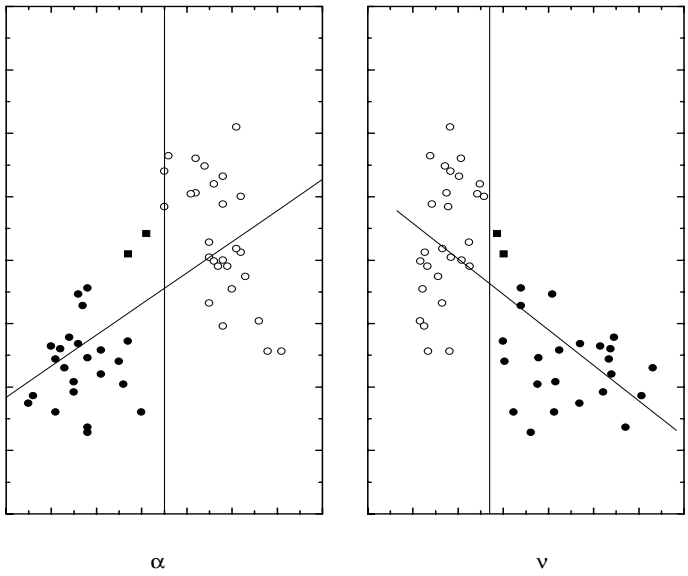

Fig. 2. a) Plot of $\log L_o - \alpha_{rx}$ for RBL and XBL samples. The empty circles represent RBLs ,solid squares represent 1652+398 and 2005−489 and the solid circles represent XBLs. The horizontal solid line is $\alpha_{rx} = 0.75$; **b)** plot of $\log L_o - \log \nu_p$ for RBL and XBL samples. The empty circles represent RBLs, solid squares represent 1652+398 and 2005−489, and the solid circles represent XBLs. The horizontal solid line is $\log \nu_p = 14.7$.

where the correlation coefficient is $r = 0.886$ and the chance probability is $p = 2.26 \times 10^{-17}$, $n = 52$. Obviously, the correlation is very strong. In this figure, four different regions are divided by the lines $\alpha_{rx} = 0.75$ and $\log L_r = 43.25$ (erg s^{-1}); all LBLs are located in the upper-right region; all HBLs are inside the lower-left region (two RBLs, 1652+398 and 2005−489 are HBLs); no sources are in the lower-right region and the upper-left region. We plot L_r versus ν_p in Fig. 1b, which shows that the radio luminosity L_r decreases as the peak frequency ν_p increases. The correlation analysis gives

$$\log L_r = -(0.67 \pm 0.06) \log \nu_p + (53.13 \pm 0.92), \quad (2)$$

where the correlation coefficient is $r = -0.841$ and the chance probability is $p = 4.42 \times 10^{-14}$, $n = 52$. The correlation is also very strong. In the four different regions divided by the lines $\log \nu_p = 14.7$ and $\log L_r = 43.25$, all LBLs are located in the upper-left region; all HBLs are inside the lower-right region (two RBLs, 1652+398 and 2005−489 are HBLs); no sources are in the lower-left region and the upper-right region.

In Fig. 2, we consider the correlation between the optical luminosity L_o and α_{rx} and that between L_o and ν_p. The results are

$$\log L_o = (2.45 \pm 0.45)\alpha_{rx} + (43.94 \pm 0.33) \quad (3)$$

with $r = 0.614$ and $p = 2.70 \times 10^{-6}$, $n = 52$ and

$$\log L_o = -(0.28 \pm 0.05) \log \nu_p + (49.93 \pm 0.68) \quad (4)$$

with $r = -0.660$ and $p = 2.52 \times 10^{-7}$, $n = 52$ respectively. It can be seen that (i) there is a positive correlation between L_o and α_{rx} and a negative correlation between L_o and ν_p, and (ii) HBLs and LBLs can be distinguished by the line of $\alpha_{rx} \approx 0.75$ (see Fig. 2a) or the line of $\log \nu_p \approx 14.7$ (see Fig. 2b), but they cannot be distinguished by optical luminosity.

Finally, we study the relation of the X-ray luminosity L_x with α_{rx} and ν_p. The correlation analysis reads

$$\log L_x = -(1.41 \pm 0.43)\alpha_{rx} + (46.08 \pm 0.32) \quad (5)$$

for L_x versus α_{rx}, where $r = -0.42$ and $p = 0.002$.

$$\log L_x = (0.11 \pm 0.05) \log \nu_p + (43.43 \pm 0.73) \quad (6)$$

for L_x versus ν_p, where $r = 0.30$ and $p = 0.03$. Obviously, there is no correlation between L_x and α_{rx} or between L_x and ν_p. We plot the results in Fig. 3. The distributions of HBLs and LBLs in the plot of L_x versus α_{rx} (Fig. 3a) and L_x versus ν_p (Fig. 3b) are confused although the lines $\alpha_x \approx 0.75$ and $\log \nu_p \approx 14.7$ can be drawn.

The results of the regression analysis are listed in Table 3.

3. Discussions and conclusions

Sambruna et al. (1996) have performed a statistical analysis of the relations of bolometric luminosity L_B (as estimated from parabolic fits to the multi-wavelength range from radio to X-ray bands) with position of the peak frequency $\log \nu_p$ and with the broad-band spectral index α_{rx} for blazars. They found that (i) there is a correlation between L_B and α_{rx} at >99% confidence, which may indicate that more luminous objects have steeper α_{rx}, and (ii) more luminous sources have smaller peak frequencies, since the average bolometric luminosity increases from XBLs to RBLs to flat spectrum radio quasars (FSRQs) on average, FSRQs are more luminous and have lower peak frequencies while XBLs are less luminous and have higher peak frequencies. In their analysis, the XBLs and RBLs are not distinguished very well in either the L_B-α_{rx} plot or L_B-ν_p plot. In this paper, we have studied the relations of radio, optical and X-ray luminosities with broad-band spectral index (α_{rx})

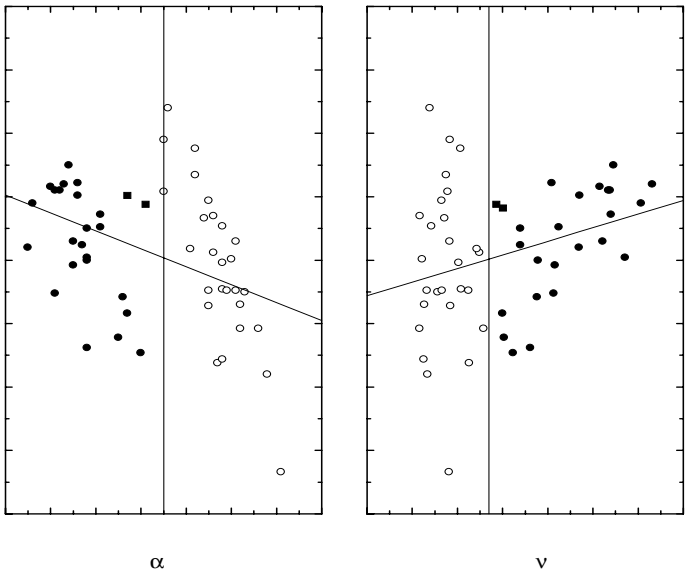

Fig. 3. a) Plot of $\log L_x - \alpha_{rx}$ for RBL and XBL samples. The empty circles represent RBLs, solid squares represent 1652+398 and 2005−489 and the solid circles represent XBLs. The horizontal solid line is $\alpha_{rx} = 0.75$. **b)** Plot of $\log L_x - \log \nu_p$ for RBL and XBL samples. The empty circles represent RBLs, solid squares represent 1652+398 and 2005−489, and the solid circles represent XBLs. The horizontal solid line is $\log \nu_p = 14.7$.

Table 3. Linear regression analysis results ($y = Ax + B, N = 52$).

y	x	A	B	r	P
$\log L_r$	α_{rx}	6.64 ± 0.49	38.24 ± 0.37	0.886	2.26×10^{-17}
$\log L_r$	$\log \nu_p$	-0.67 ± 0.06	53.13 ± 0.92	−0.841	4.42×10^{-14}
$\log L_o$	α_{rx}	2.45 ± 0.45	43.94 ± 0.33	0.614	2.70×10^{-6}
$\log L_o$	$\log \nu_p$	-0.28 ± 0.05	49.93 ± 0.68	−0.660	2.52×10^{-7}
$\log L_x$	α_{rx}	-1.41 ± 0.43	46.08 ± 0.32	−0.42	0.002
$\log L_x$	$\log \nu_p$	0.11 ± 0.05	43.43 ± 0.73	0.30	0.03

r denotes the correlation coefficient and P denotes the chance probability.

and peak frequency (ν_p) for 52 BL Lac objects (including 23 XBLs and 29 RBLs). It is different from the analysis of Sambruna et al. (1996); we analyzed the relation of luminosity at each energy band to α_{rx} and ν_p, respectively.

From our analysis, we found that radio luminosity L_r can be used to distinguish HBLs and LBLs. Our results indicate that there is a very strong positive correlation between L_r and α_{rx} and a negative correlation between L_r and ν_p. More importantly, HBLs and LBLs can be distinguished very well in both the L_r–α_{rx} plot (see Fig. 1a) and L_r–ν_p plot (see Fig. 1b). We have also analyzed the relations of the optical and X-ray luminosities with α_{rx} and ν_p, respectively. We found that the optical luminosity has a good correlation with both α_{rx} and ν_p (see Figs. 2a and b), but X-ray luminosity shows no correlation with α_{rx} or ν_p (see Figs. 3a and b). Obviously, neither L_o or L_x can be used to distinguish HLBs and LBLs. Therefore, α_{rx}, ν_p and L_r are equivalent in the classifications of HBLs and LBLs: HBLs fall in the region divided by the lines of $\alpha_{rx} \leq 0.75$ (or $\log \nu_p > 14.7$ Hz) and $\log L_r \leq 43.25$ erg s^{-1} while LBLs fall in the region divided by the lines of $\alpha_{rx} > 0.75$ (or $\log \nu_p \leq 14.7$ Hz) and $\log L_r > 43.25$ erg s^{-1}.

It is known that the observed spectral energy distributions of BL Lac objects show a peak between IR and X-rays, and the most likely radiation mechanism is synchrotron radiation. In Fig. 1a of the L_r and α_{rx} plot, HBLs are distributed in the region divided by the lines of $\alpha_{rx} \leq 0.75$ and $\log L_r \leq 43.25$ erg s^{-1}. Using the definition of α_{rx} and $\alpha_{rx} \leq 0.75$, we have $\log L_x \geq \log L_r + 1$ erg s^{-1} for HBLs where $\nu_r = 5$ GHz and $\nu_x = 1$ keV are used. Since $\log L_r \leq 43.25$ erg s^{-1}, we have $\log L_x \geq 44.25$ erg s^{-1} for HBLs while $\log L_x < 44.25$ erg s^{-1} for LBLs. Compared to the result shown in Fig. 3a, the observed X-ray luminosities of HBLs in our sample are above the lower limit of $\log L_x \geq 44.25$ erg s^{-1}, indicating that X-rays from HBLs are produced by synchrotron radiation. From Fig. 3a, we see that the observed X-ray luminosities for most LBLs do not satisfy the upper limit of $L_x < 44.25$ erg s^{-1}. We believe that inverse Compton scattering provides more important contributions to X-ray emission from these LBLs.

Finally, we would like to point out that we have performed the analysis of the relation of energy fluxes at radio, optical and X-ray bands with α_{rx} and ν_p. We find that radio energy flux can distinguish HBLs and LBLs very well.

Acknowledgements. The Special Funds for Major State Basic Project of China (Grant No. 2000077602), the National 973 project of China (Grant No. NKBRAFG19990754), the Natural Science Foundation of China and the Natural Science Foundation of Yunnan province of China are acknowledged for financial support. We would like to thank Dr. J. H. Fan for useful discussions.

References

Dong, Y. M., Mei, D. C., & Liang, E. W. 2002, PASJ, 54, 171
Falomo, R., Scarpa, R., & Bersanelli, M. 1994, ApJS, 93, 125
Fossati, G., Maraschi, L., Celotti, A., Comastri, A., & Ghisellini, G. 1998, MNRAS, 299, 433
Ghisellini, G., Maraschi, L., Treves, A., & Tanzi, E. G. 1986, ApJ, 310, 317
Giommi, P., & Padovani, P. 1994, MNRAS, 268, L51
Giommi, P., Ansari, S. G., & Micol, A. 1995, A&AS, 109, 267
Giommi, P., Barr, P., Pollock, A. M. T., Garilli, B., & Maccagni, D. 1990, ApJ, 356, 432
Lamer, G., Brunner, H., & Staubert, R. 1996, A&A, 311, 384
Landau, R., Golisch, B., Jones, T. J., et al. 1986, ApJ, 308, 78
Ledden, J. E., & O'Dell, S. L. 1985, ApJ, 298, 630
Maraschi, L., Ghisellini, G., & Celotti, A. 1992, ApJ, 397, L5
Padovani, P., & Giommi, P. 1995, ApJ, 444, 567
Padovani, P., & Giommi, P. 1996, MNRAS, 279, 526
Qin, Y. P., Xie, G. Z., & Zheng, X. T. 1999, Ap&SS, 266, 549
Sambruna, R. M., Maraschi, L., & Urry, C. M. 1996, ApJ, 463, 444
Schachter, J. F., Stocke, J. T., Perlman, E., et al. 1993, ApJ, 412, 541
Stocke, J. T., Liebert, J., Schmidt, G., et al. 1985, ApJ, 298, 619
Stocke, J. T., Morris, S. L., Gioia, I. M., et al. 1991, ApJS, 76, 813
Urry, C. M., & Padovani, P. 1995, PASP, 107, 803